ARTICLE

A polarity-induced defect mechanism for conductivity and magnetism at polar–nonpolar oxide interfaces

Liping Yu[1,2] & Alex Zunger[1]

The discovery of conductivity and magnetism at the polar–nonpolar interfaces of insulating nonmagnetic oxides such as $LaAlO_3$ and $SrTiO_3$ has raised prospects for attaining interfacial functionalities absent in the component materials. Yet, the microscopic origin of such emergent phenomena remains unclear, posing obstacles to design of improved functionalities. Here we present first principles calculations of electronic and defect properties of $LaAlO_3/SrTiO_3$ interfaces and reveal a unifying mechanism for the origins of both conductivity and magnetism. We demonstrate that the polar discontinuity across the interface triggers thermodynamically the spontaneous formation of certain defects that in turn cancel the polar field induced by the polar discontinuity. The ionization of the spontaneously formed surface oxygen vacancy defects leads to interface conductivity, whereas the unionized Ti-on-Al antisite defects lead to interface magnetism. The proposed mechanism suggests practical design principles for inducing and controlling both conductivity and magnetism at general polar–nonpolar interfaces.

[1] Office of the Vice Chancellor for Research, University of Colorado, Boulder, Colorado 80309, USA. [2] Materials and Engineering Science Program, University of Colorado, Boulder, Colorado 80309, USA. Correspondence and requests for materials should be addressed to L.Y. (email: yuliping@gmail.com).

O xide interfaces exhibit many spectacular phenomena not found in the respective bulk components or in conventional semiconductor interfaces[1], providing new avenues for electronics[2]. The LaAlO$_3$/SrTiO$_3$ interface is a paradigm example, exhibiting conducting two-dimensional (2D) electron gas (2DEG)[3,4] and magnetism[5–11] between two insulating nonmagnetic metal oxides. In the [001] direction, two different interfaces can be formed between polar LaAlO$_3$, which consists of alternating LaO)$^+$–(AlO$_2$)$^-$ layers, and nonpolar SrTiO$_3$, which consists of alternating (SrO)^0–(TiO$_2$)^0 layers. One is LaO/TiO$_2$ stacking configuration (so-called n-type) and the other is AlO$_2$/SrO configuration (so-called p-type). The remarkable feature is that the conductivity occurs only at n-type interfaces when the LaAlO$_3$ film thickness (n_{LAO}) is larger than three unit cells (uc)[4,5], whereas the magnetism has been observed both at n-type interfaces with $n_{LAO} > \sim 3$ uc and at insulating p-type interfaces[8]. Table 1 lists some experimental observations representing the main puzzles[12] that need to be resolved before the promised applications can be realized[13].

For 2DEG at n-type interfaces, four main mechanisms have been suggested, yet no single one explains the full scope of these puzzles. The prevalent one is intrinsic electronic reconstruction (so-called polar catastrophe) involving ionization of the electrons from host valence band of LaAlO$_3$ within the abrupt and defect-free interfaces (Supplementary Fig. 1)[3,4]. The other three mechanisms involve various defects, including the oxygen vacancies at the interface (denoted as $V_O(I)$, where 'I' means 'Interface')[14–16], oxygen vacancies at LaAlO$_3$ overlayer surface (denoted as $V_O(S)$, where S means 'Surface')[17–22], and the La-on-Sr (La$_{Sr}$) antisite donor defects induced by interfacial cation intermixing[23–29]. As Table 1 shows, each of these proposed mechanisms represents one aspect of the interface physics, explains some experimental findings, but conflicts with a few others[2]. None explains the insulating nature of p-type interfaces. Regarding interface magnetism, it was shown experimentally that the local magnetic moments are associated with Ti^{3+} ions[5–11,30]. However, it is yet unclear whether such Ti^{3+} ions reside in the interface within SrTiO$_3$ side, or LaAlO$_3$ side, or both sides. Theoretically, it has been argued that the Ti^{3+} ions arise in SrTiO$_3$ side, owing to the occupation of the low-energy Ti-d_{xy}-like sub-bands caused by the interfacial splitting of orbital degeneracy[31], or interfacial disorder[32,33], or interfacial oxygen vacancies[34]. However, these scenarios are difficult to explain the fact that magnetism occurs at p-type interfaces and n-type interfaces with a critical thickness (L_c) similar to that for 2DEG.

The centrosymmetric III–III–O$_3$ perovskite has a non-zero formal polarization, as established by the modern theory of polarization[35,36]. The discontinuity in the formal polarization of

LaAlO$_3$ and SrTiO$_3$ leads to a finite polar field that would cause the divergence of electrostatic potential as the n_{LAO} increases. A crucial issue associated with the emergent conductivity and magnetism at polar–nonpolar interfaces is what mitigates such potential divergence. Is it electronic reconstruction within the polar catastrophe scenario, or the atomic reconstruction scenario with or without chemical defects? Different mechanisms suggest different experimental designs that would control conductivity, mobility and magnetism. Particularly, for defects, it is unclear which defects can be induced and are responsible for the emergent interface phenomena. Using first principles electronic and defect calculations, we find that the certain defects would form spontaneously in response to the built-in polar field. The ensuing polarity-induced defect mechanism (Fig. 1) simultaneously explains the main features of both conductivity and magnetism at the interface, as summarized in Table 2.

The key defect-related physical quantities that feature in our explanation are (i) the formation energy ΔH of defects in various charge states (q) at the thermodynamic equilibrium Fermi energy E_F (Fig. 2). This ΔH controls the equilibrium defect concentration; (ii) the defect charge transition energy levels (deep or shallow; Fig. 3), $\varepsilon(q/q')$ defined as the E_F where the ΔH of a defect in two different charge states q and q' equal. A donor can produce electrons and compensate holes, whereas an acceptor can produce holes and compensate electrons. These two quantities (i) and (ii) calculated for charged defects located in different layers across the interfaces turn out to be crucial. The details of their first principles calculations are given in the Methods section.

The central point of the proposed mechanism is that the polar-discontinuity-induced built-in polar field triggers thermo dynamically the spontaneous formation of certain defects at the surface and/or interface, which in turn compensate the built-in polar field and thus avoids the potential divergence. Thus, it is the polar-field-induced defects, rather than the electronic or atomic reconstruction, that are responsible for the conductivity and magnetism at the interface. Specifically, we find that the surface V_O has its donor levels located energetically above the SrTiO$_3$ conduction band at the interface but below the LaAlO$_3$ conduction band. This donor level position is a prerequisite for 2DEG formation. Although the occurring of the 2DEG is because of the surface donors, the density of 2DEG is controlled by the interfacial deep acceptor defects (mainly Al-on-Ti antisite). It has also turned out that the interface magnetic moment is caused by the unionized deep Ti-on-Al antisite defects located within the LaAlO$_3$ side near the interface.

We address below how this polar-field-induced defect mechanism resolves the long-standing puzzles on the origin of 2DEG, the critical thickness for 2DEG, the weak field in LaAlO$_3$

Table 1 | List of some important experimental observations at LaAlO$_3$/SrTiO$_3$ interfaces.

Interface structure	Experimental observations	Polar catastrophe	Cation mixing	V_O at interface	V_O at surface	Current mechanism
n-type	Critical thickness (L_c) = 4 uc	✔	X	X	?	✔
	2DEG density $< 0.5e\ S_{2D}^{-1}$[1]	X	?	X	X	✔
	Weak E in LaAlO$_3$ for $n_{LAO} < L_c$	X	?	X	X	✔
	Weak E in LaAlO$_3$ for $n_{LAO} \geq L_c$	X	X	X	✔	✔
	LaAlO$_3$ surface: insulating	X	?	?	✔	✔
	Interface: cation intermixed	X	✔	X	X	✔
	Interface magnetism	X	?	X	X	✔
p-type	Interface: insulating	X	?	X	?	✔
	LaAlO$_3$ surface: insulating	X	X	?	?	✔
	Interface: cation mixed	X	✔	X	X	✔
	Interface magnetism	X	?	?	X	✔

The symbol of '✔' and 'X' mean that the mechanism agrees or disagrees, respectively, with the experimental observation. The '?' symbol denotes uncertainty.

film, the density of 2DEG, the insulating nature of p-type interfaces and the origin of the local magnetic moments. During this process, we also distil the general design principles that control the pertinent effects and could allow future section of better polar–nonpolar interface materials.
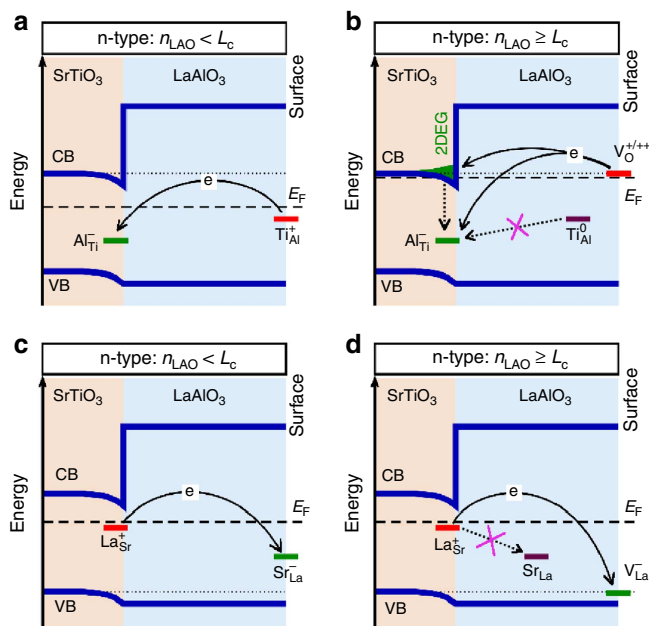

Figure 1 | Schematic band diagram and change transfer among the defects at LaAlO$_3$/SrTiO$_3$ interfaces. (**a**) n-type interfaces with $n_{LAO} < L_c$: all electrons transferred from Ti$_{Al}$(S) are trapped by deep Al$_{Ti}$(I), causing no 2DEG. (**b**) n-type interfaces with $n_{LAO} \geq L_c$: V$_O$(S) defects donate ~ 0.5 e S$_{2D}^{-1}$ to the interface. Part of ~ 0.5 e S$_{2D}^{-1}$ is trapped by the Al$_{Ti}$(I) and the rest leads to interfacial 2DEG. The formed Ti$_{Al}$ defects are ionized, i.e., Ti^{3+}-on-Al^{3+}, having local magnetic moments. (**c,d**) p-type interfaces with $n_{LAO} < L_c$ (~ 4 uc) and $n_{LAO} \geq L_c$: all electrons transferred from La$_{Sr}$(I) are trapped by Sr$_{La}$(S) and V$_{La}$(S), respectively. All involved defects are deep and do not induce carriers. The un-ionized Ti$_{Al}^0$ (not shown in **c,d**) also form and induce local moments. The superscripts $(0, +, ++, -)$ in the Figure denote the defect charge states, not the oxidation states of the ions there.

Results

The origin of the 2DEG. The 2DEG is unlikely to originate from the defect-free scenarios: these include the ionization of the intrinsic LaAlO$_3$ valence bands (suggested by the polar catastrophe model[3,4]) or the ionization of the LaO interface layer (suggested by the interfacial charge-leaking model)[37] (Supplementary Note 1). This conclusion stems from the fact that the creation of 2DEG in these defect-free scenarios requires the LaAlO$_3$ valence band maximum (VBM) to cross the SrTiO$_3$ conduction band minimum (CBM) or E_F. However, this is contrary to the experimentally observed weak field (negligible band-bending)[38–41] in the LaAlO$_3$ film, clearly showing that the LaAlO$_3$ VBM is located energetically far below the E_F.

The 2DEG also is unlikely to originate from interfacial point donor defects (La$_{Sr}$, Ti$_{Al}$ and V$_O$). Recall first that the defect formation energy (ΔH) depends on the E_F (or chemical potential) and the defect charge transition energy $\varepsilon(q/q')$ needs to be close to band edges in order to produce free carriers. In thermodynamic equilibrium, the E_F of the system pins around the middle of SrTiO$_3$ band gap when $n_{LAO} < L_c$ and around the SrTiO$_3$ conduction band edge near the interface when $n_{LAO} \geq L_c$ (Supplementary Note 2). In either case, Fig. 2ab shows that the ΔH of the interfacial antisite donor defects, La$_{Sr}^0$ and Ti$_{Al}^0$, is small positive or even negative (note: the superscript denotes the defect charge states, not the nominal oxidation state of the atom at the defect site). In other words, the formation of such antisite defects at the thermodynamic equilibrium E_F is energetically favourable and would inevitably lead to interfacial cation mixing. However, at such E_F, both La$_{Sr}^0$ and Ti$_{Al}^0$ defects are stable in their charge neutral states (as indicated by the superscript), contributing no free carriers. On the other hand, the interfacial V$_O$ defects are energetically stable in the charged states, that is, V$_O^{2+}$ (Fig. 2a,b). This means that, if formed, the V$_O$ will donate electrons and thereby become positively charged. However, the ΔH of V$_O^{2+}$ at such equilibrium E_F is rather high (> 2.5 eV), implying that V$_O^{2+}$ have very low concentration under thermodynamic equilibrium conditions. The high ΔH also means that even if the V$_O$ defects are formed under nonequilibrium growth conditions, they can still be removed easily by the post O-rich annealing process[42] (Supplementary Note 3). Thus, contrary to earlier postulations, these interfacial donor defects are not responsible for 2DEG, consistent with recent experiments[43].
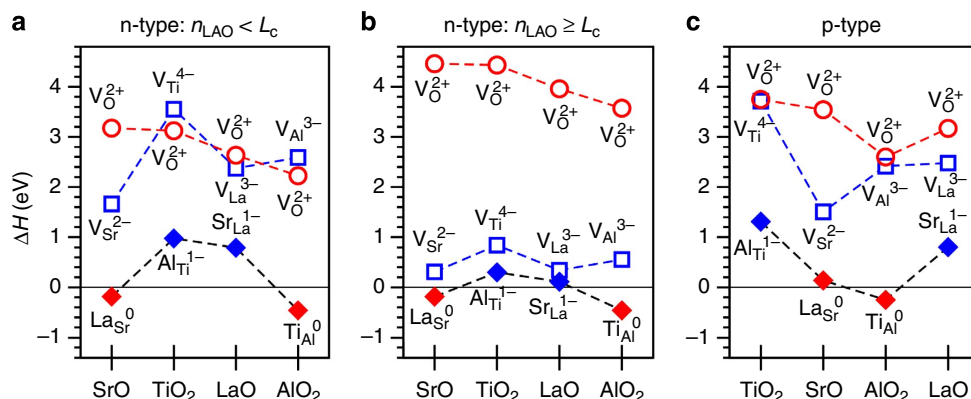

Figure 2 | Formation energy of the interfacial point defects at thermodynamical equilibrium Fermi energy. (**a,b**) n-type interfaces with $n_{LAO} < L_c$ and $n_{LAO} \geq L_c$, respectively. (**c**) p-type interfaces. At a given E_F, the defect in different charge states (for example, V$_{Sr}^0$, V$_{Sr}^{1-}$, V$_{Sr}^{2-}$) usually has different ΔH and the only one with the lowest ΔH is shown in the Figure. The ΔH versus E_F for these defects are shown in Supplementary Fig. 2, which also includes other high-ΔH defects not shown here. The chemical potentials used for Sr, Ti, La, Al and O are -4.36, -6.20, -6.10, -5.46 and -2.0 eV, respectively, relative to their corresponding elemental solid or gas phases, which corresponds to $T = 1050$ K and $P_{O2} = 6.1 \times 10^{-6}$ Torr (Supplementary Fig. 3).
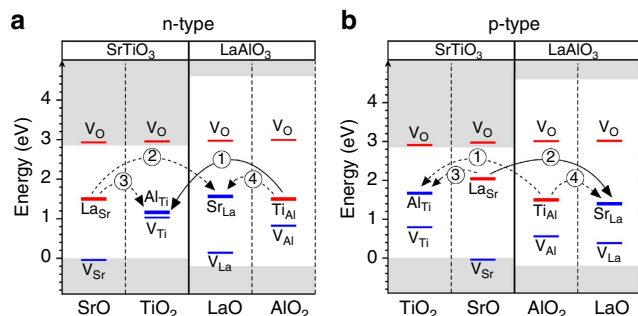
Figure 3 | Charge transition energy levels of the interfacial point defects.
(**a**) n-type interface. (**b**) p-type interface. The defect charge transition energy level is defined as the E_F where the ΔH of a given defect in two different charge states equal. Some defects may have multiple charge transition energy levels. For example, V_{Sr} has the two transition energy levels (one is for the transition between neutral charge state and -1, and the other is between -1 and -2). In such case, if the defect is donor (red), only the lowest level is shown, and if the defect is acceptor (blue), the highest level is shown.

The oxygen vacancy, $V_O(S)$, at the free $LaAlO_3$ surface can explain the interfacial 2DEG. For this to happen, three conditions ('design principles') need to be satisfied. First, $V_O(S)$ in the polar film material needs to have a sufficiently low formation energy ΔH; therefore, it could form in significant quantities. Figure 4a shows that the ΔH of $V_O(S)$ decreases linearly as the film thickness n_{LAO} increases, consistent with previous calculations[20,44]. When $n_{LAO} \geq 3$–4 uc, the ΔH becomes zero or negative, and $V_O(S)$ will form spontaneously. The large negative ΔH means that even exposing the surface to air or post annealing under O-rich environment cannot remove these vacancies. Second, the system needs to have a none-zero built-in polar field that would enable the electron to transfer from the surface of the polar material to the interface. Such transfer sets up an opposite dipole (proportional to n_{LAO}), which in turn cancels the field and lowers the ΔH. The larger the n_{LAO}, the lower the ΔH. Note that in the absence of such field, the surface-to-interface charge transfer would not occur since such a transfer would create a dipole that would increase the electrostatic energy (proportional to that dipole) and thus raise the total energy of the system. Third, the donor transition level of $V_O(S)$ in the polar film should be higher in energy than in the substrate ($SrTiO_3$) conduction band edge at the interface (Fig. 3). These three conditions are satisfied in this $LaAlO_3/SrTiO_3$ system.

It is noteworthy that it is the built-in polar field that triggers the spontaneous formation of the $V_O(S)$ when $n_{LAO} \geq L_c$. Such built-in polar field always exists in the $LaAlO_3$ to be grown during the layer-by-layer growth. This is because that the surface defects (here V_O) can cancel the built-in polar field only in the $LaAlO_3$ film between the interface and the surface, not the built-in polar field in the $LaAlO_3$ film to be grown on top of the surface.

In the absence of interfacial defects, the emerging picture for creating 2DEG is that the electrons ionized from $V_O(S)$ of the polar film material transfer to the nonpolar substrate material $SrTiO_3$ conduction bands at the interface via the built-in polar field, thus forming the 2DEG at that interface. This charge transfer in turn cancels the built-in polar field in $LaAlO_3$, which caused the low ΔH of the surface vacancies in the first place. After the built-in field has been cancelled, the ΔH of $V_O(S)$ return to a high value (>3 eV) characteristic of the bulk, and $V_O(S)$ become again hard to form in thermodynamic equilibrium[20]. Thus, the theoretical maximum concentration of $V_O(S)$ is $0.25\, S_{2D}^{-1}$ (where S_{2D} is 2D unit cell area), that is, one of eight oxygen missing at

surface. These would donate maximally $0.5e\, S_{2D}^{-1}$ that would completely cancel the polar field in $LaAlO_3$. The compensation of polar field by $V_O(S)$ also means that the band bending in $LaAlO_3$ because of polar field is removed. Thus, the $LaAlO_3$ valence bands fall well below the E_F, contrary to what the polar catastrophe model would suggest. Consequently, no free holes can arise from depopulation of the $LaAlO_3$ valence bands at the surface, consistent with experiments[3,22].

The emerging design principles for selecting materials that will form interfacial 2DEG are: (i) the nonpolar material needs to have a CBM positioned in the band gap of the polar material; (ii) the polar material needs to have at least one donor defect with its donor level higher in energy than the conduction band of the nonpolar material at the interface. This picture suggests that the 2DEG at n-type $LaAlO_3/SrTiO_3$ interfaces may also be induced and/or tuned by using certain surface adsorbates (for example, H_2O and H)[45–47] or metallic contacts[48] provided that the ionization energy of the surface adsorbate or the metallic contact is not lower than the donor level of the $V_O(S)$.

The origin of the critical thickness. The linear decrease in ΔH of $V_O(S)$ with increasing polar film thickness n_{LAO} naturally explains the critical thickness L_c for the metal–insulator transition. The calculated rate of decrease (that is, the slope $d\Delta H/dn_{LAO}$) equals 0.19 eV Å^{-1}, which is the same as the calculated built-in polar field in the defect-free $LaAlO_3$ film (Supplementary Note 4). The $V_O(S)$ defects start to form spontaneously when the ΔH becomes zero at the L_c of ~ 4 uc under a typical O-rich growth condition (Fig. 4a). For the $LaAlO_3$ film that is 1 uc thinner than this L_c, the calculated ΔH of $V_O(S)$ is 0.75 eV, which is too high to produce significant free carrier concentration. Thus, the appearance of $V_O(S)$ (and the ensuing metal–insulator transition) at L_c is predicted to be a sharp transition (Supplementary Note 5), distinct from the gradual appearance of 2DEG behaviour as predicted from polar catastrophe model, but consistent with experiments[49].

Figure 3a suggests that the L_c resulting from $V_O(S)$ can be written as $L_c = \Delta H_o/eE_p$, where ΔH_o is the formation energy of the V_O at interface (or the ΔH extrapolated at $n_{LAO} = 0$) and E_p is the built-in polar field. Using $E_p = 4\pi P_0/\epsilon$ (where ϵ and P_0 are the dielectric constant and formal polarization of $LaAlO_3$ film), this relation can be written as

$$L_c = \Delta H_o \epsilon / 4\pi e P_0 \qquad (1)$$

which predicts an L_c of ~ 4 uc, depending slightly on the O-poor/rich growth conditions (Supplementary Note 6). The above formula provides an alternative explanation for the observed variation of the L_c with the fraction x in $(LaAlO_3)_{1-x}(SrTiO_3)_x$ overlayer (where P_0 is proportional to x)[50]. This observation was originally explained by $L_c = \Delta\Phi/4\pi e P_0$ (where $\Delta\Phi$ is the energy difference between $LaAlO_3$ VBM and $SrTiO_3$ CBM) within polar catastrophe model[50]. Since $\Delta\Phi$ and ΔH_o have accidentally similar value (~ 3–4 eV) in this system, it is not surprising that the L_c predicted from these two models is also similar. However, the $V_O(S)$ model clearly explains many other observations in which the polar catastrophe model fails (Table 1).

Implication on the design of carrier mobility: (i) the relatively high 2DEG mobility could be enabled by a modulated doping effect[51], whereby the source of carriers (here at the $LaAlO_3$ surface) is spatially separated from the location where the carriers reside (here at the $LaAlO_3/SrTiO_3$ interface), thus minimizing carrier scattering by the ionized defects. This minimal spatial separation is measured by the critical thickness L_c. The equation (1) suggests that a large L_c (hence maintaining good mobility) could be achieved by selecting a polar materials with small polarization, large dielectric constant and donor defects
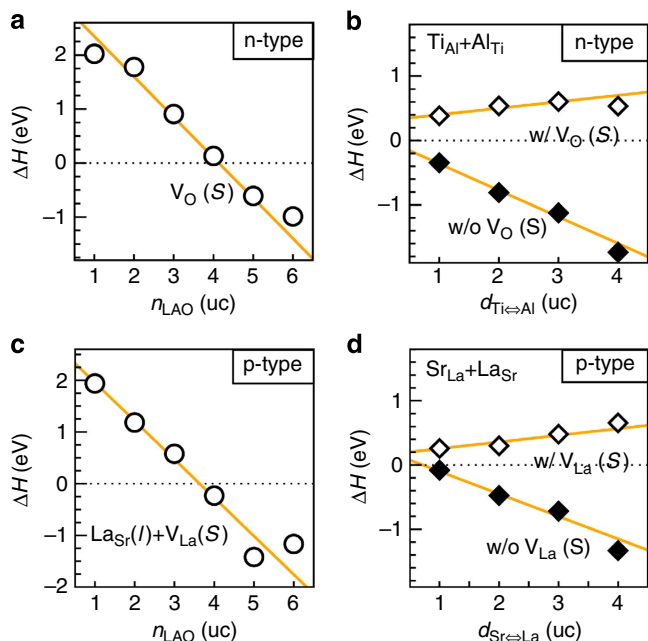
Figure 4 | Properties of surface defects and defect complexes. (a) The GGA-calculated ΔH of $V_O(S)$ defect, under the O-rich growth condition (that is, $\Delta\mu_O = -1.5$ eV, Supplementary Fig. 3a). **(b)** the ΔH of $[Ti_{Al} + Al_{Ti}]$ defect pair created from a Ti⇔Al exchange out of the ideal interface with and without a $V_O(S)$ in a 2×2 $(SrTiO_3)_6/(LaAlO_3)_4/vacuum$ surpercell. **(c)** The GGA-calculated ΔH of $[La_{Sr}(I) + V_{La}(S)]$ defect complex as a function of n_{LAO}, under $\Delta\mu_{Sr} = -4.36$ eV (Supplementary Fig. 3b). **(d)** the ΔH of $[La_{Sr} + Sr_{La}]$ defect pair created from a La⇔Sr exchange out of the ideal interface with and without a $V_{La}(S)$ in a 2×2 $(SrTiO_3)_6/(LaAlO_3)_4/$ vacuum surpercell, respectively. The $d_{Ti\Leftrightarrow Al}$ and $d_{La\Leftrightarrow Sr}$ in **b,d** are the distance between the components of corresponding defect pair. The orange lines are the guides to the eye.

having high ΔH at the interface or in the bulk. On the other hand, (ii) the concentration of interfacial defects must be minimized in order to take advantage of (i). In addition, (iii) since the 2DEG is located at the conduction bands of the nonpolar material, it is advantageous to select the nonpolar material with low electron effective mass in order to achieve higher mobility.

Polar field compensation. Experimentally, only very weak residual field has been observed in the $LaAlO_3$ film no matter whether its thickness is below or above the L_c (refs 38–41,52). This observation cannot be explained within the defect-free interface scenario, even including the ionic relaxations[53]. In turn, whereas the $V_O(S)$ model explains the weak electric field in $LaAlO_3$ film above the L_c, it does not explain it below the L_c. This leads us to inspect the effects of all possible cation antisite defects across the interface.

Each individual interfacial antisite alone cannot cancel the polar field. Figure 2ab shows that the La_{Sr}, Sr_{La}, Ti_{Al} and Al_{Ti} antisite defects have lower ΔH than other point defects (for example, cation vacancies) in the layer where they are located. Therefore, the former are the dominant defects in their corresponding layers. The interfacial La_{Sr} donor in the $SrTiO_3$ side cannot set up an opposite dipole across the $LaAlO_3$ film that can cancel the polar field inside the $LaAlO_3$ film. Regarding the Ti_{Al} donor in the $LaAlO_3$ side, the donor level is lower than the $SrTiO_3$ conduction band at the interface. Therefore, the ionized electrons cannot be transferred to the latter so as to cancel the

polar field. Regarding the interfacial Al_{Ti} and Sr_{La} acceptors, the polar field compensation is similar to that in the polar catastrophe model: before the $LaAlO_3$ VBM reaches the acceptor levels of Al_{Ti} or Sr_{La}, the polar field cannot be cancelled.

The $[Ti_{Al} + Al_{Ti}]$ defect pair is the most potent source of polar field cancellation among those donor–acceptor antisite defect pairs at n-type interfaces. The four leading antisite defects can form four types of donor–acceptor pairs: $[Ti_{Al} + Al_{Ti}]$, $[La_{Sr} + Sr_{La}]$, $[La_{Sr} + Al_{Ti}]$ and $[Ti_{Al} + Sr_{La}]$, denoted as ①, ②, ③ and ④, respectively, in Fig. 3. Clearly, the electron transfer from donor to acceptor in both pairs ② and ③ is unlikely since it will create a dipole in the same direction as the intrinsic dipole in $LaAlO_3$, and thus increase the dipole moment (also the electrostatic energy) and destabilize the interface. In pairs ① and ④, the charge transfer can cancel the polar field. However, the electron transfer in pair ① is energetically much more favourable because, first, Al_{Ti} has a lower acceptor level than Sr_{La} and, second, the donor–acceptor separation distance (also the associated opposite dipole moment that lowers the total energy of the system) is larger in pair ① (Fig. 3a). We thus next focus on $[Ti_{Al} + Al_{Ti}]$ (that is, pair ①).

For $n_{LAO} < L_c$, the $[Al_{Ti} + Ti_{Al}]$ antisite pair can form spontaneously via Ti⇔Al exchange across the interface and cancel the polar field. Figure 4b (filled symbols) shows that the energy required to form such defect pair is negative (that is, exothermic), and the largest energy gain is obtained when a Ti atom of TiO_2-interface monolayer is exchanged with an Al of AlO_2-surface monolayer, that is, $Al_{Ti}(I) + Ti_{Al}(S)$, which is consistent with previous first principles calculations[54]. This means that Ti atom at the interface would hop to the AlO_2-surface layer and exchange with Al atom there. Similar to the case of $V_O(S)$, the linear decrease in ΔH with increasing donor–acceptor separating distance (Fig. 4b) is a sign of polar field compensation. Indeed, the electron transfer from the Ti_{Al} donor to the Al_{Ti} acceptor is expected, since the donor level is higher in energy than the acceptor level (Fig. 3a). Figure 4a also shows that the $V_O(S)$ has too high ΔH to form for $n_{LAO} < L_c$ (Fig. 4a). Therefore, the polar field is cancelled by those spontaneously formed $[Al_{Ti}(I) + Ti_{Al}(S)]$ pairs. On the other hand, since these defects are deep, they cannot cause free carriers in the both interface and surface regions (whence insulating).

For $n_{LAO} \geq L_c$, the polar field is cancelled by spontaneously formed $V_O(S)$, not by $[Al_{Ti}(I) + Ti_{Al}(S)]$. Recall that the polar field always exists in the $LaAlO_3$ layers during the layer-by-layer growth. Such polar field can trigger the formation of $V_O(S)$ and/ or $Ti_{Al}(S)$ defects as n_{LAO} increases. For $n_{LAO} \geq L_c$, both $V_O(S)$ (Fig. 4a) and $[Al_{Ti}(I) + Ti_{Al}(S)]$ pair (Fig. 4b) have zero or negative ΔH, meaning that both could form in ideal interfaces. However, if both $V_O(S)$ and $Ti_{Al}(S)$ are present, since V_O has an energetically higher donor level than Ti_{Al} (Fig. 3a), the $V_O(S)$ would transfer electrons to the Ti_{Al} defects. The polar field that was initially cancelled by the electrons transferred from the Ti_{Al} defects are then released and get cancelled by the electrons transferred from $V_O(S)$ defects. Consequently, the polar field in the whole $LaAlO_3$ film would be cancelled by the $V_O(S)$ defects (if present). The larger the n_{LAO}, the lower the ΔH of the $V_O(S)$. After the polar field has been cancelled by $V_O(S)$, Fig. 4b (open symbols) shows that the ΔH of $[Al_{Ti}(I) + Ti_{Al}(S)]$ pair becomes positive (0.4–0.7 eV), meaning that $[Ti_{Al} + Al_{Ti}]$ pairs cannot be formed via Ti⇔Al exchange over a distance beyond L_c. In brief, the presence of the $[Ti_{Al} + Al_{Ti}]$ defect pairs in the sample does not change the linear-decreasing behaviour in the ΔH of the $V_O(S)$ (Fig. 4a), suggesting that the metal–insulator transition still occurs at the L_c of ~ 4 uc. However, the presence of $V_O(S)$ would prevent $[Ti_{Al} + Al_{Ti}]$ pairs forming further above the L_c, and reduce the concentration of these pairs formed below the L_c.

The density of the 2DEG. Reinterpretation of the puzzle: According to Gauss' law, the experimentally observed weak electric field in LaAlO$_3$ film means that the total external charge density (mobile and/or immobile) at the interface must be $\sim 0.5e$ S_{2D}^{-1} (Supplementary Note 7), as recently observed[55]. For $n_{LAO} < L_c$, there is no interfacial conductivity and thus none of these interfacial charge contribute to the conductivity. For $n_{LAO} \geq L_c$, only a fraction of $0.5e$ S_{2D}^{-1} interfacial charge is seen in transport, and so the majority of $0.5e$ S_{2D}^{-1} charges do not contribute to the conductivity. The puzzle thus is why the $\sim 0.5e$ S_{2D}^{-1} charge exists at the interface with any n_{LAO}, but only a small part of it contributes to conducting 2DEG when $n_{LAO} \geq L_c$.

This puzzle cannot be explained by defect-free polar cata-strophe model[3,4] or interfacial charge-leaking model[37], since both predict zero interfacial charge for $n_{LAO} < L_c$ and an interfacial charge density much higher than the measured 2DEG density for $n_{LAO} \geq L_c$ (Supplementary Fig. 1). The possibility of 'multiple carrier types' at defect-free interfaces (that is, those electrons occupying interfacial d_{xy} sub-band and those occupying d_{xz}/d_{yz} sub-bands contribute differently in transport) has also been suggested to explain the measured 2DEG density above the L_c (refs 56–59). However, this scenario could not explain the total $0.5e$ S_{2D}^{-1} interface charge that is independent of n_{LAO}. Moreover, it is also difficult to explain why a full carrier density of $0.5e$ S_{2D}^{-1} has been observed at GdTiO$_3$/SrTiO$_3$ interfaces (where the same multiple carrier types exist)[60].

The 2DEG density is controlled by the concentration of immobile acceptor defects that can trap itinerant electrons. Within the emerging defect picture, the total interfacial charge is always $\sim 0.5e$ S_{2D}^{-1}, which corresponds to the (almost) complete polar field cancellation. In the SrTiO$_3$ side (where the 2DEG is located), there are mainly three types of acceptor defects, namely, Al$_{Ti}$, V$_{Sr}$ and V$_{Ti}$. At equilibrium E_F, Fig. 2a,b shows that these acceptor defects all prefer to stay in negative charge states, that is, Al$_{Ti}^{1-}$, V$_{Sr}^{2-}$ and V$_{Ti}^{4-}$. (In other defect charge states, these defects have much higher ΔH and are not shown in Fig. 2a,b.). This means that once these defects form they will trap free electrons from the system and get negatively charged. Among these acceptor defects, the Al$_{Ti}^{1-}$ acceptors have the lowest ΔH and thus they the most potent electron-trapping agents. For $n_{LAO} < L_c$, the Al$_{Ti}$ defects resulting from Ti $\Leftrightarrow$ Al exchange trap all free electrons transferred from Ti$_{Al}(S)$ defects, and hence no free carrier can occur. For $n_{LAO} \geq L_c$, the ΔH of [Ti$_{Al}$ + Al$_{Ti}$] pair changes from negative to positive because of V$_O(S)$ (Fig. 4b), meaning that the concentration of Al$_{Ti}$ defect resulting from Ti $\Leftrightarrow$ Al exchange is reduced, compared with that formed below the L_c. Therefore, the Al$_{Ti}$ defect concentration is not sufficient to trap all $0.5e$ S_{2D}^{-1} electrons transferred from V$_O(S)$. Therefore, only a small fraction of $0.5e$ S_{2D}^{-1} can contribute to interface 2DEG.

The recently observed LaAlO$_3$ cation-stoichiometry effect on 2DEG formation[43] may also be understood within the above picture. For Al-rich LaAlO$_3$ film, where both A-site and B-site sublattices are fully occupied (hence having no cation vacancies), the Al$_{Ti}$ antisites are the only electron-trapping defects and the incomplete trapping of $0.5e$ S_{2D}^{-1} interface charge by Al$_{Ti}$ defects leads to interface conductivity. However, for La-rich LaAlO$_3$ film, where B-site sublattice is not fully occupied, the cation vacancies (V$_{Ti}$ and V$_{Al}$) also become the main electron-trapping agents, in addition to Al$_{Ti}(I)$. Although the concentration of Al$_{Ti}$ is reduced, each cation vacancy induced in the La-rich film traps more electrons than an Al$_{Ti}$. The insulating character can thus be then attributed to the complete interfacial electron trapping by both interfacial cation vacancies and Al$_{Ti}$ (I).

The picture of Al$_{Ti}(I)$ as the main electron-trapping agent may be extended to SrTiO$_3$/GdTiO$_3$ interfaces. The observed full

carrier density of $0.5e$ S_{2D}^{-1} there[60] can be ascribed to the fact that both SrTiO$_3$ and GdTiO$_3$ have the same Ti atom at B-site sublattice and thus have no Al$_{Ti}$-like antisite defects at the interface.

Implication on how to increase the density of 2DEG: The above picture suggests that the main controlling factor for the interface carrier density is the concentration of the acceptor defects (mainly Al$_{Ti}$ in stoichiometric or Al-rich film), which should be minimized for enhancing carrier density. Such Al$_{Ti}$-like electron-trapping defects may be completely removed by designing other oxide interfaces such as GdTiO$_3$/SrTiO$_3$ interfaces, whose bulk components have a common cation atom with multiple valence states.

The origin of the insulting nature of p-type interfaces. An intriguing fact is that the so-called p-type interfaces are not p-type (hole) conducting but are actually insulating. The defect-free polar-catastrophe model for p-type interface predicts a hole-conducting interface and an electron-conducting surface when $n_{LAO} > \sim 7.3$ uc (Supplementary Fig. 1) in contradiction with the insulating behaviour observed robustly in experiment. To explain this, defects must be involved. The emerging defect picture below differs from the literature model based solely on interfacial hole–polaron[61] or interfacial hole-compensating V$_O$ defects[23,44], which assumes that the interface has holes arising from the depopulation of the intrinsic SrTiO$_3$ valence bands.

Individual point defects alone at p-type interfaces can neither cause conductivity nor cancel the polar field. As was the case for n-type interfaces, Fig. 2b shows that the interfacial La$_{Sr}$ and Ti$_{Ar}$ are stable at their charge neutral states and have negligible or negative ΔH at equilibrium E_F. This means that they cause inevitable interfacial cation intermixing but induce no free carriers. The V$_O$ and other defects at the interface require too high ΔH to form, and thus they do not produce free carriers either. For similar reason, each of the leading antisite defects (La$_{Sr}$, Sr$_{La}$, Ti$_{Al}$ and Al$_{Ti}$) alone at p-type interfaces cannot cancel the polar field.

The spontaneously formed donor–acceptor defect pairs always cancel the polar field but do not induce free carriers. Among the four donor–acceptor defect pairs as indicted in Fig. 3b, the [La$_{Sr}$ + Sr$_{La}$] (that is, pair ②) is energetically most favourable to cause polar field cancellation. For $n_{LAO} < \sim 4$ uc, the [La$_{Sr}(I)$ + Sr$_{La}(S)$] pairs have negative ΔH (Fig. 4d) and can form spontaneously via La $\Leftrightarrow$ Sr exchanges, whereas the [La$_{Sr}(I)$ + V$_{La}(S)$] have too high ΔH to form (Fig. 4c). Therefore, the polar field is cancelled by the charge transfer from La$_{Sr}(I)$ to Sr$_{La}(S)$, which can be expected from their relative defect levels (Fig. 3b) and their linear decreasing behaviour in ΔH as a function of n_{LAO} (Fig. 4d). For $n_{LAO} \geq \sim 4$ uc, the ΔH of [La$_{Sr}(I)$ + V$_{La}(S)$] become negative (Fig. 4c) and can also form spontaneously. Since V$_{La}$ has a lower acceptor level than Sr$_{La}$ (Fig. 3b), the polar field is cancelled by the charge transfer from La$_{Sr}(I)$ to V$_{La}(S)$, rather than to Sr$_{La}(S)$. In absence of an electric field, Fig. 4d (open symbols) indicates that the La $\Leftrightarrow$ Sr exchanges cannot occur anymore over a distance of ~ 4 uc. Unlike the case in n-type interfaces, the V$_O(S)$ defects in p-type interface always have too high ΔH to form. The defects involved in polar field cancellation are all deep. The calculated equilibrium E_F according to those point defects turns out to be always around the middle of SrTiO$_3$ band gap. This means that both VBM and CBM are far away from the E_F, and there are no free carrier arising from the depopulation of VBM and CBM in both interface and surface regions (whence insulating).

Implication on the design of 2D hole conductivity: Clearly, the formation of interfacial free holes is prevented by these

spontaneously formed deep La_{Sr} defects that have donor level higher than the VBM at the interface. Therefore, to induce interfacial hole conductivity, one should search for the polar–nonpolar interfaces where all such donors have high enough formation energy to form or (ii) their donor levels below the VBM at the interface. Practically, the (ii) may be achieved more easily by searching for the polar material whose VBM is higher than the charge transition energy levels of those spontaneously formed interfacial donor defects.

The origin of interface magnetism. Distinct from previous models[31–34] that explain magnetism based on the intrinsic interfacial Ti^{3+} ion in the $SrTiO_3$ (that is, not a defect), we find below that the local magnetic moment originates from the unionized deep Ti_{Al} antisite defect (that is, Ti^{3+}-on-Al^{3+} within $LaAlO_3$ side near the interface. The interface magnetism depends on the concentration and spatial distribution of such Ti_{Al} defects. This picture explains not only why the magnetism appears at n-type interfaces with a similar critical thickness to that for 2DEG but also why the magnetism also appears at insulating p-type interfaces[8].

What causes local moment? As discussed earlier, for n-type interfaces, when $n_{LAO} < L_c$, the polar field in $LaAlO_3$ is cancelled by the charge transfer from $Ti_{Al}(S)$ defects to the interface. These formed Ti_{Al} defects are thus ionized, that is, Ti_{Al}^{1+} (where superscript denotes the defect charge states). The Ti ion at this defect site has the oxidation states of $4+$, denoted as Ti^{4+}, which has no local magnetic moment. Moreover, noted before, when $n_{LAO} \geq L_c$, the polar field in $LaAlO_3$ is cancelled by the charge transfer to the interface from $V_O(S)$ instead of Ti_{Al}. In absence of internal field, all $Ti_{Al}(I)$ defects in the $LaAlO_3$ film are most stable in their charge neutral (or unionized) states, that is, Ti_{Al}^0, where Ti appears as Ti^{3+} oxidation state, having a finite local magnetic moment. Therefore, the interface magnetism at n-type interfaces because of those unionized Ti_{Al}^0 defects should also have a critical thickness of ~ 4 uc. For p-type interfaces, it is the charge transfer among the defects other than Ti_{Al} defects that cancels the polar field in $LaAlO_3$. Thus, all Ti_{Al} defects formed there are not ionized, having local magnetic moments, and cause interface magnetism.

The magnitude of local magnetic moment: The local moment of a single Ti_{Al} defect at the interface can be estimated from that in bulk $LaAlO_3$, which is $0.84\mu_B$ from our hybrid functional calculation. For ferromagnetic order as observed in the experiment, the total interface magnetic moment depends on the concentration of unionized Ti_{Al} defects in $LaAlO_3$ and can be

very small per Ti atom in average. The experimentally observed inhomogeneous landscape of magnetism that also varies from sample to sample[8,9] may be attributed to the various spatial distributions of Ti_{Al} defects, which may be sensitive to sample preparation conditions (such as temperature and P_{O2}) and local strain.

The $Ti_{Al}(I)$ defects within LaAlO side being the origin of the local moment are more reasonable than $V_O(I)$ in two aspects. First, the deep Ti_{Al} defect is spatially localized and has an unambiguous local moment. In contrast, V_O is a shallow donor that transfer electrons to the lower-energy interfacial Ti d_{xy} sub-bands that have light effective mass inside the interface plane[59]; therefore, the resulting Ti^{3+} may then be itinerant. Second, the Ti_{Al} defects would form readily because of the small or negative ΔH of Ti_{Al}, whereas the interfacial V_O requires significant energy to form and if formed it may be removed completely after annealing.

Discussion

We establish a physical link between polar discontinuity and defect formation: the polar discontinuity triggers spontaneous formation of certain defects that in turn cancel the polar field induced by polar discontinuity. It is the subtle interplay of those spontaneously formed surface vacancy defects and interfacial cation antisite defects that control the physics of the system by their formation energies and relative defect levels. Table 2 summarizes how those defects shown in Fig. 1 explain the leading experimental observations and puzzles in Table 1. The explanation leads to a set of design principles for both conductivity and magnetism at $LaAlO_3/SrTiO_3$ and other polar–nonpolar interfaces and enables the design of better polar–nonpolar interfaces.

Having ruled out the electronic reconstruction, interfacial V_O and interfacial cation intermixing mechanism as the possible origin of 2DEG in our calculations, we conclude that the 2DEG at n-type interfaces with $n_{LAO} \geq L_c$ originates from the spontaneously formed $V_O(S)$ defects. This conclusion stems from the finding that the donor level of deep V_O in the $LaAlO_3$ side is higher than the $SrTiO_3$ conduction band edge at the interface. This finding explains why the formation energy of $V_O(S)$ decreases linearly as n_{LAO} increases. This linear decrease relation leads to some new controlling parameters for the critical thickness of sharp metal–insulator transition in absence of the electric field in the polar $LaAlO_3$ film. Instead of causing the 2DEG, the anti site defect pair turns out to play a key role in canceling the polar field, controlling the density of the 2DEG, and inducing the local magnetic moments at the interface (Table 2).

The emerging mechanism provides three distinctive predictions to be tested in experiment as further validation. (i) For

Table 2 | The specific defects and their charge transfer processes that explain the leading experimental observations at stoichiometric $LaAlO_3/SrTiO_3$ interfaces.

	n-type interface structure		p-type interface structure	
	$n_{LAO} < L_c$	$n_{LAO} \geq L_c$	$n_{LAO} < L_c$	$n_{LAO} \geq L_c$
Polar field compensation	$Ti_{Al}(S) \rightarrow Al_{Ti}(I)$	$V_O(S) \rightarrow Al_{Ti}(I)$ and $V_O(S) \rightarrow CBM(I)$	$La_{Sr}(I) \rightarrow Sr_{La}(S)$	$La_{Sr}(I) \rightarrow V_{La}(S)$
Origin of 2DEG/2DHG	No 2DEG: $Al_{Ti}(I)$ traps all electrons from $Ti_{Al}(S)$	$V_O(S) \rightarrow CBM(I)$: $Al_{Ti}(I)$ traps part of electrons from $V_O(S)$	No 2DHG: $La_{Sr}(I)$ traps all holes from $Sr_{La}(S)$	No 2DHG: $La_{Sr}(I)$ traps all holes from $V_{La}(S)$
Density of 2DEG/2DHG	Zero	< 0.5 e S_{2D}^{-1}	Zero	Zero
Origin of critical thickness	Polar-field induced $V_O(S)$ formation		Polar-field induced $V_{La}(S)$ formation	
Origin of interface magnetism	Ti^{4+}-on-Al^{3+} forms but has no local moment	Ti^{3+}-on-Al^{3+} forms and induces local moment	Ti^{3+}-on-Al^{3+} forms and induces local moment	Ti^{3+}-on-Al^{3+} forms and induces local moment

The "S" and "I" denote the $LaAlO_3$ free surface and $LaAlO_3/SrTiO_3$ interface, respectively. S_{2D} is the two-dimensional unit cell area.

n-type interfaces, the AlO_2-surface layer is dominated by Ti_{Al} defects when $n_{LAO} < L_c$ and by V_O defect when $n_{LAO} \geq L_c$. (ii) For p-type interfaces, the LaO-surface layer is dominated by Sr_{La} and V_{La} defects, respectively, below and above an L_c of ~ 4 uc. (iii) Ti^{4+} and Ti^{3+} signals exist in both sides of the interface. The appearance of the Ti^{3+} signals should not be taken as a sign of conductivity. Whether the Ti^{3+} signals detected by photoemission below the L_c (refs 21,40,62,63) can be truly assigned to those Ti^{3+} ions in the $SrTiO_3$ side should be revisited carefully. How these Ti_{Al} local moments are ordered (ferromagnetic, or antiferromagnetic, or else) and whether and how they interact with the itinerant 2DEG are still open questions that should be investigated further.

Methods

Computational techniques. All calculations were performed using density functional theory and plane-wave projector-augmented wave[64] method as implemented in the VASP code[65]. An energy cutoff of 400 eV was used. The Brillouin zone was sampled by $8 \times 8 \times 1$ and $4 \times 4 \times 1$ **k**-point mesh for 1×1 and 2×2 in-plane supercell, respectively. The atomic forces were relaxed to be less than $0.03\,eV\,Å^{-1}$. The in-plane lattice constant was fixed to $3.943\,Å$ (the relaxed lattice constant of $SrTiO_3$ by GGA[66]). In slab calculations, the 4-uc ($\sim 16\,Å$) vacuum layer was used and the dipole correction was always applied to remove artificial dipole interactions[67]. The results in Figs 2 and 3 were obtained by using HSE hybrid functional[68] on top of the GGA-relaxed structures.

First principles defect theory. The formation energy of a defect (D) calculated from $\Delta H_D^q(E_F, \mu) = E_D^q - E_H + \sum_\alpha n_\alpha (\mu_\alpha^0 + \Delta\mu_\alpha) + q(E_v + E_F)$, where E_D^q and E_H are the total energies of a supercell with and without defect, respectively, and D is in charge state q. n_α is the number of atoms of species α needed to create a defect. E_F is the Fermi energy relative to VBM (E_v). $\Delta\mu_\alpha$ is the relative chemical potential of species α with respect to its elemental solid (gas; μ^0). The equilibrium Fermi energy was calculated self-consistently according to charge neutrality condition[69]. The chemical potentials relative to their elemental solid (or gas) phase are taken as variables and are bounded by the values that maintain a stable host compound and avoid the formation of other competing phases in thermodynamic equilibrium (Supplementary Fig. 3). The details of theory and calculations can be found in ref. 70.

References

1. Hwang, H. Y. *et al.* Emergent phenomena at oxide interfaces. *Nat. Mater.* **11**, 103–113 (2012).
2. Mannhart, J. & Schlom, D. G. Oxide interfaces-an opportunity for electronics. *Science* **327**, 1607–1611 (2010).
3. Ohtomo, A. & Hwang, H. Y. A high-mobility electron gas at the $LaAlO_3$/$SrTiO_3$ heterointerface. *Nature* **427**, 423–426 (2004).
4. Thiel, S., Hammerl, G., Schmehl, A., Schneider, C. W. & Mannhart, J. Tunable quasi-two-dimensional electron gases in oxide heterostructures. *Science* **313**, 1942–1945 (2006).
5. Brinkman, A. *et al.* Magnetic effects at the interface between non-magnetic oxides. *Nat. Mater.* **6**, 493–496 (2007).
6. Li, L., Richter, C., Mannhart, J. & Ashoori, R. C. Coexistence of magnetic order and two-dimensional superconductivity at $LaAlO_3$/$SrTiO_3$ interfaces. *Nat. Phys.* **7**, 762–766 (2011).
7. Ariando *et al.* Electronic phase separation at the $LaAlO_3$/$SrTiO_3$ interface. *Nat. Commun.* **2**, 188 (2011).
8. Kalisky, B. *et al.* Critical thickness for ferromagnetism in $LaAlO_3$/$SrTiO_3$ heterostructures. *Nat. Commun.* **3**, 922 (2012).
9. Salman, Z. *et al.* Nature of weak magnetism in $SrTiO_3$/$LaAlO_3$ multilayers. *Phys. Rev. Lett.* **109**, 257207 (2012).
10. Lee, J. S. *et al.* Titanium d(xy) ferromagnetism at the $LaAlO_3$/$SrTiO_3$ interface. *Nat. Mater.* **12**, 703–706 (2013).
11. Joshua, A., Ruhman, J., Pecker, S., Altman, E. & Ilani, S Gate-tunable polarized phase of two-dimensional electrons at the $LaAlO_3$/$SrTiO_3$ interface. *Proc. Natl Acad. Sci. USA* **110**, 9633–9638 (2013).
12. Chen, H. H., Kolpak, A. M. & Ismail-Beigi, S. Electronic and magnetic properties of $SrTiO_3$/$LaAlO_3$ interfaces from first principles. *Adv. Mater.* **22**, 2881–2899 (2010).
13. Chakhalian, J., Millis, A. J. & Rondinelli, J. Whither the oxide interface. *Nat. Mater.* **11**, 92–94 (2012).
14. Siemons, W. *et al.* Origin of charge density at $LaAlO_3$ on $SrTiO3$ heterointerfaces: Possibility of intrinsic doping. *Phys. Rev. Lett.* **98**, 196802 (2007).
15. Kalabukhov, A. *et al.* Effect of oxygen vacancies in the $SrTiO3$ substrate on the electrical properties of the $LaAlO_3$/$SrTiO_3$ interface. *Phys. Rev. B* **75**, 121404 (2007).
16. Herranz, G. *et al.* High mobility in $LaAlO_3$/$SrTiO_3$ heterostructures: Origin, dimensionality, and perspectives. *Phys. Rev. Lett.* **98**, 216803 (2007).
17. Cen, C. *et al.* Nanoscale control of an interfacial metal-insulator transition at room temperature. *Nat. Mater.* **7**, 298–302 (2008).
18. Zhong, Z. C., Xu, P. X. & Kelly, P. J. Polarity-induced oxygen vacancies at $LaAlO_3$/$SrTiO_3$ interfaces. *Phys. Rev. B* **82**, 165127 (2010).
19. Bristowe, N. C., Littlewood, P. B. & Artacho, E. Surface defects and conduction in polar oxide heterostructures. *Phys. Rev. B* **83**, 205405 (2011).
20. Li, Y., Phattalung, S. N., Limpijumnong, S., Kim, J. & Yu, J. Formation of oxygen vacancies and charge carriers induced in the n-type interface of a $LaAlO_3$ overlayer on $SrTiO_3(001)$. *Phys. Rev. B* **84**, 245307 (2011).
21. Takizawa, M., Tsuda, S., Susaki, T., Hwang, H. Y. & Fujimori, A. Electronic charges and electric potential at $LaAlO_3$/$SrTiO_3$ interfaces studied by core-level photoemission spectroscopy. *Phys. Rev. B* **84**, 245124 (2011).
22. Berner, G. *et al.* Direct k-space mapping of the electronic structure in an oxide-oxide interface. *Phys. Rev. Lett.* **110**, 247601 (2013).
23. Nakagawa, N., Hwang, H. Y. & Muller, D. A. Why some interfaces cannot be sharp. *Nat. Mater.* **5**, 204–209 (2006).
24. Willmott, P. R. *et al.* Structural basis for the conducting interface between $LaAlO_3$ and $SrTiO_3$. *Phys. Rev.* **99**, 155502 (2007).
25. Kalabukhov, A. S. *et al.* Cationic disorder and phase segregation in $LAALO_3$/$SRTIO_3$ heterointerfaces evidenced by medium-energy ion spectroscopy. *Phys. Rev. Lett.* **103**, 146101 (2009).
26. Yamamoto, R. *et al.* Structural comparison of n-type and p-type $LaAlO_3$/$SrTiO_3$ interfaces. *Phys. Rev. Lett.* **107**, 036104 (2011).
27. Qiao, L., Droubay, T. C., Kaspar, T. C., Sushko, P. V. & Chambers, S. A. Cation mixing, band offsets and electric fields at $LaAlO_3$/$SrTiO_3(001)$ heterojunctions with variable La:Al atom ratio. *Surf. Sci.* **605**, 1381–1387 (2011).
28. Vonk, V. *et al.* Polar-discontinuity-retaining A-site intermixing and vacancies at $SrTiO_3$/$LaAlO_3$ interfaces. *Phys. Rev. B* **85**, 045401 (2012).
29. Gunkel, F. *et al.* Influence of charge compensation mechanisms on the sheet electron density at conducting $LaAlO_3$/$SrTiO_3$-interfaces. *Appl. Phys. Lett.* **100**, 052103 (2012).
30. Salluzzo, M. *et al.* Origin of interface magnetism in $BiMnO_3$/$SrTiO_3$ and $LaAlO_3$/$SrTiO3$ heterostructures. *Phys. Rev. Lett.* **111**, 087204 (2013).
31. Banerjee, S., Erten, O. & Randeria, M. Ferromagnetic exchange, spin-orbit coupling and spiral magnetism at the $LaAlO_3$/$SrTiO_3$ interface. *Nat. Phys.* **9**, 625–629 (2013).
32. Fidkowski, L., Jiang, H. C., Lutchyn, R. M. & Nayak, C. Magnetic and superconducting ordering in one-dimensional nanostructures at the $LaAlO_3$/$SrTiO_3$ interface. *Phys. Rev. B* **87**, 014436 (2013).
33. Michaeli, K., Potter, A. C. & Lee, P. A. Superconducting and ferromagnetic phases in $SrTiO_3$/$LaAlO_3$ oxide interface structures: possibility of finite momentum pairing. *Phys. Rev. Lett.* **108**, 117003 (2012).
34. Pavlenko, N., Kopp, T., Tsymbal, E. Y., Mannhart, J. & Sawatzky, G. A. Oxygen vacancies at titanate interfaces: two-dimensional magnetism and orbital reconstruction. *Phys. Rev. B* **86**, 064431 (2012).
35. Resta, R. & Vanderbilt, D. in *Physics of Ferroelectrics: a Modern Perspective (eds Rabe, K M., Ahn, C. H. & Triscone, J.-M.) 31–68 (Springer-Verlag, 2007)*.
36. Stengel, M. & Vanderbilt, D. Berry-phase theory of polar discontinuities at oxide-oxide interfaces. *Phys. Rev. B* **80**, 241103 (2009).
37. Janotti, A., Bjaalie, L., Gordon, L. & Van de Walle, C. G. Controlling the density of the two-dimensional electron gas at the $SrTiO_3$/$LaAlO_3$ interface. *Phys. Rev. B* **86**, 241108 (2012).
38. Segal, Y., Ngai, J. H., Reiner, J. W., Walker, F. J. & Ahn, C. H. X-ray photoemission studies of the metal-insulator transition in $LaAlO_3$/$SrTiO_3$ structures grown by molecular beam epitaxy. *Phys. Rev. B* **80**, 241107 (2009).
39. Huang, B. C. *et al.* Mapping band alignment across complex oxide heterointerfaces. *Phys. Rev. Lett.* **109**, 246807 (2012).
40. Slooten, E. *et al.* Hard x-ray photoemission and density functional theory study of the internal electric field in $SrTiO_3$/$LaAlO_3$ oxide heterostructures. *Phys. Rev. B* **87**, 085128 (2013).
41. Berner, G. *et al.* Band alignment in $LaAlO_3$/$SrTiO_3$ oxide heterostructures inferred from hard x-ray photoelectron spectroscopy. *Phys. Rev. B* **88**, 115111 (2013).
42. Van de Walle, C. G. & Neugebauer, J. First-principles calculations for defects and impurities: applications to III-nitrides. *J. Appl. Phys.* **95**, 3851–3879 (2004).
43. Warusawithana, MP *et al.* $LaAlO_3$ stoichiometry is key to electron liquid formation at $LaAlO_3$/$SrTiO_3$ interfaces. *Nat. Commun.* **4**, 2351 (2013).
44. Zhang, L. X. *et al.* Origin of insulating behavior of the p-type $LaAlO_3$/$SrTiO_3$ interface: Polarization-induced asymmetric distribution of oxygen vacancies. *Phys. Rev. B* **82**, 125412 (2010).
45. Xie, Y. W., Hikita, Y., Bell, C. & Hwang, H. Y. Control of electronic conduction at an oxide heterointerface using surface polar adsorbates. *Nat. Commun.* **2**, 494 (2011).
46. Bi, F. *et al.* "Water-cycle" mechanism for writing and erasing nanostructures at the $LaAlO_3$/$SrTiO_3$ interface. *Appl. Phys. Lett.* **97**, 173110 (2010).

47. Son, W. J., Cho, E., Lee, J. & Han, S. Hydrogen adsorption and carrier generation in LaAlO₃-SrTiO₃ heterointerfaces: a first-principles study. *J. Phys. Condens. Mater.* **22,** 315501 (2010).

48. Arras, R., Ruiz, V. G., Pickett, W. E. & Pentcheva, R. Tuning the two-dimensional electron gas at the LaAlO₃/SrTiO₃(001) interface by metallic contacts. *Phys. Rev. B* **85,** 125404 (2012).

49. Liu, Z. Q. *et al.* Origin of the two-dimensional electron gas at LaAlO₃/SrTiO₃ interfaces: the role of oxygen vacancies and electronic reconstruction. *Phys. Rev. X* **3,** 021010 (2013).

50. Reinle-Schmitt, M. L. *et al.* Tunable conductivity threshold at polar oxide interfaces. *Nat. Commun.* **3,** 932 (2012).

51. Dingle, R., Stormer, H. L., Gossard, A. C. & Wiegmann, W. Electron mobilities in modulation-doped semiconductor heterojunction super-lattices. *Appl. Phys. Lett.* **33,** 665–667 (1978).

52. Liang, H. X. *et al.* Giant photovoltaic effects driven by residual polar field within unit-cell-scale LaAlO₃ films on SrTiO₃. *Sci. Rep. Uk* **3,** 1975 (2013).

53. Pentcheva, R. & Pickett, W. E. Avoiding the polarization catastrophe in LaAlO₃ overlayers on SrTiO₃(001) through polar distortion. *Phys. Rev. Lett.* **102,** 107602 (2009).

54. Chambers, S. A. *et al.* Instability, intermixing and electronic structure at the epitaxial LaAlO₃/SrTiO₃(001) heterojunction. *Surf. Sci. Rep.* **65,** 317–352 (2010).

55. Asmara, T. C. *et al.* Mechanisms of charge transfer and redistribution in LaAlO₃/SrTiO₃ revealed by high-energy optical conductivity. *Nat. Commun.* **5,** 3663 (2014).

56. Popovic, Z. S., Satpathy, S. & Martin, R. M. Origin of the two-dimensional electron gas carrier density at the LaAlO₃ on SrTiO₃ interface. *Phys. Rev. Lett.* **101,** 256801 (2008).

57. Son, W. J., Cho, E., Lee, B., Lee, J. & Han, S. Density and spatial distribution of charge carriers in the intrinsic n-type LaAlO₃-SrTiO₃ interface. *Phys. Rev. B* **79,** 245411 (2009).

58. Seo, S. S. A. *et al.* Multiple conducting carriers generated in LaAlO₃/SrTiO₃ heterostructures. *Appl. Phys. Lett.* **95,** 082107 (2009).

59. Delugas, P. *et al.* Spontaneous 2-dimensional carrier confinement at the n-type SrTiO₃/LaAlO₃ interface. *Phys. Rev. Lett.* **106,** 166807 (2011).

60. Moetakef, P. *et al.* Electrostatic carrier doping of GdTiO3/SrTiO3 interfaces. *Appl. Phys. Lett.* **99,** 232116 (2011).

61. Pentcheva, R. & Pickett, W. E. Charge localization or itinerancy at LaAlO₃/SrTiO₃ interfaces: Hole polarons, oxygen vacancies, and mobile electrons. *Phys. Rev. B* **74,** 035112 (2006).

62. Sing, M. *et al.* Profiling the interface electron gas of LaAlO₃/SrTiO₃ heterostructures with hard X-ray photoelectron spectroscopy. *Phys. Rev. Lett.* **102,** 176805 (2009).

63. Park, J. *et al.* Oxygen-vacancy-induced orbital reconstruction of Ti ions at the interface of LaAlO₃/SrTiO₃ heterostructures: a resonant soft-X-ray scattering study. *Phys. Rev. Lett.* **110,** 017401 (2013).

64. Blochl, P. E. Projector augmented-wave method. *Phys. Rev. B* **50,** 17953–17979 (1994).

65. Kresse, G. & Furthmuller, J. Efficiency of ab-initio total energy calculations for metals and semiconductors using a plane-wave basis set. *Comp. Mater. Sci.* **6,** 15–50 (1996).

66. Perdew, J. P., Burke, K. & Ernzerhof, M. Generalized gradient approximation made simple. *Phys. Rev. Lett.* **77,** 3865–3868 (1996).

67. Yu, L. P., Ranjan, V., Lu, W., Bernholc, J. & Nardelli, M. B. Equivalence of dipole correction and Coulomb cutoff techniques in supercell calculations. *Phys. Rev. B* **77,** 245102 (2008).

68. Heyd, J., Scuseria, G. E. & Ernzerhof, M. Hybrid functionals based on a screened Coulomb potential (vol 118, pg 8207, 2003). *J. Chem. Phys.* **124,** 219906 (2006).

69. Persson, C., Zhao, Y. J., Lany, S. & Zunger, A. n-type doping of CuInSe₂ and CuGaSe₂. *Phys. Rev. B* **72,** 035211 (2005).

70. Freysoldt, C. *et al.* First-principles calculations for point defects in solids. *Rev. Mod. Phys.* **86,** 253 (2014).

Acknowledgements

Author contributions

L.Y. carried out the calculations, analysed the results and wrote the paper. A.Z. initiated the study of this topic and contributed to the analysis of the results and to the writing of the paper.

Additional information

Supplementary Information accompanies this paper at http://www.nature.com/naturecommunications

Competing financial interests: The authors declare no competing financial interests.

Reprints and permission information is available online at http://npg.nature.com/reprintsandpermissions/

How to cite this article: Yu, L. *et al.* A polarity-induced defect mechanism for conductivity and magnetism at polar–nonpolar oxide interfaces. *Nat. Commun.* 5:5118 doi: 10.1038/ncomms6118 (2014).